J Mater Sci (2011) 46:832–838
DOI 10.1007/s10853-010-4825-5

Adhesives with patterned sub-surface microstructures

Edward Peter Arul · Animangsu Ghatak

Received: 11 May 2010 / Accepted: 10 August 2010 / Published online: 21 August 2010

Abstract Inspired by the complex hierarchical structures found in natural adhesives, we have embedded monolithic stack of several microchannels inside soft layers of silicon elastomers. These channels are rectangular in cross-section and their internal surfaces are textured with microscopic pillars arranged in regular arrays. Displacement controlled indentation experiment on these adhesives shows that adhesion and debonding occur not only on the surface of the adhesive but also at the interfaces of the embedded layers. These textures on the channel surface enhance adhesion via "crack arrest and initiation" mechanism. Furthermore, the adhesive is treated by hydrochloric acid so that the siloxane bonds present on the exposed surfaces are hydrolyzed generating silanol groups which on two contacting surfaces increase the effect of self adhesion hysteresis. Thus, the combined effect of surface texturing is integrated with the chemical treatment to increase adhesion.

Introduction

Bio-mimicking of natural adhesives have been a subject of much interest because of many interesting and technologically important characteristics of these adhesives. Natural adhesive pads at the foot of many insects and vertebrates such as geckos have complex hierarchical structures consisting of surface hairs and patterns [1–8] and subsurface microstructures such as liquid filled vesicles [9] and granular secretion glands [10–12]. It is now well understood that these patterns at the surface of the adhesive enhance adhesive strength by "crack arrest and initiation" mechanism [13–19]. The adhesive strength increases also when the local modulation of the adhesive is altered by changing the capillary pressure inside the subsurface fluidic vessels [20]. Besides, adhesive strength has been enhanced via also chemical treatment, for example, by altering the surface chemistry [21–24] of the adhesive. However, generating hierarchical febrile structures of the adhesive has so far not resulted in any significant enhancement of adhesion [25].

In contrast, we generate thin elastomeric films of poly(dimethylsiloxane) (PDMS) in which we embed monolithic stack of rectangular microchannels with micropatterned walls. Displacement controlled indentation on these adhesives shows that, in addition to the contact between the indenter and the adhesive surface, sub-surface contact occurs between the walls of the microchannels resulting in significant increase in the effective area of adhesion. Furthermore, because of the presence of the patterns, the crack arrest and initiation mechanism becomes effective at each contacting interface thereby resulting in increase in hysteresis. In order to further enhance the hysteretic effect, the adhesive films are treated with dilute hydrochloric acid which hydrolyzes the siloxane bonds at the PDMS surface without altering the elastic modulus of the material. The silanol groups, thus generated at the contacting surfaces, interact with each other resulting in "self adhesion hysteresis" as described in reference [22]. During indentation experiments, adhesion occurs at the internal walls of each microchannel thereby increasing this hysteresis many fold. We have systematically varied the geometric lengthscale of the patterns to examine their effect on adhesion hysteresis.

E. P. Arul · A. Ghatak (✉)
Department of Chemical Engineering, Indian Institute of Technology, Kanpur, UP 208016, India
e-mail: aghatak@iitk.ac.in

Materials and methods

The adhesive films were prepared by using commercially available poly(dimethylsiloxane) (PDMS), the Dow Corning product sylgard-170 elastomer. Transparency sheets of known thickness were used as the template for generating the microchannels. Solvents such as acetone was used for swelling the cross linked elastomer. The photoresist SU8-2015, SU8-2035, and SU8 developer solution purchased from Microchem Corporation was used for preparing photolithographic patterns on the template material.

The microchannels were embedded inside the PDMS films by template assisted method described in references [21, 26]. Figure 1i–iii shows the preparation of templates used for the generation of microchannels inside the PDMS film. The templates were generated using thin rectangular strips of transparency sheet of thickness 100 μm and width 2 mm (Fig. 1i); these strips were first coated with SU-8 photoresist material using a spin coater (Fig. 1ii). The photoresist material was cured followed by patterning by exposing to UV by SF-100 maskless lithography system to achieve regular patterns on the surface of the templates. The template surface had the negative pattern of the positive replica of what was finally generated at the surface of the internal wall of the microchannels (Fig. 1iii).

Figure 2a–e shows the preparation of microchannel embedded inside adhesive film. The spacers of required thickness were used to control the distance between the adhesive surface and the embedded microchannel and also between the layers of microchannels arranged in a vertical stack. Figure 2a depicts such a stack of templates and spacers placed inside a pool of sylgard-170 prepolymer liquid which was cross linked between two rigid glass plates at a temperature 80 °C for 1 h (Fig. 2b). Both glass plates were coated with a monomolecular layer of octadecyltrichlorosilane (OTS) which favors easy removal of the plates after the polymer is cross linked. The cross linked sample was swelled in acetone (Fig. 2c) after which the templates were removed from the swollen block by applying a gentle pull. This process leaves a positive replicate of the patterns on the walls of the microchannel as shown in the Fig. 2d. Figure 2f shows the schematic diagram of the side view of the adhesive film with smooth and textured microchannel walls.

The skin thickness, t, interchannel spacing, h_s, channel height, h_c, and the channel width, w, were kept constant throughout the experiment: $t = h_s = 440$ μm, $h_c = 100$ μm and $w = 2$ mm; the number of channels, n, in the stack and the pillar dimensions were varied systematically; height, $h_p = 15$–60 μm, the width of the cross-section $a = 15$–67 μm, and inter pillar spacing, $s = 15$–77 μm.

The crosslinked blocks of PDMS were chemically treated by immersing the samples in dilute hydrochloric acid (pH: 1.7) for 24 h followed by rinsing thoroughly with

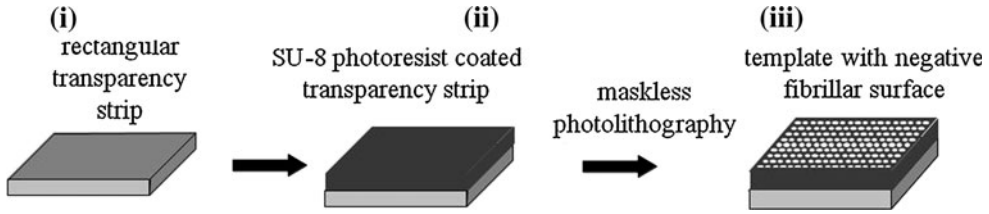

Fig. 1 Preparation of templates for generating microchannels inside the adhesive film. (*i*)–(*iii*) shows the process of generating patterns on the surface of the templates which is used for generating the stack of microchannels within the adhesive

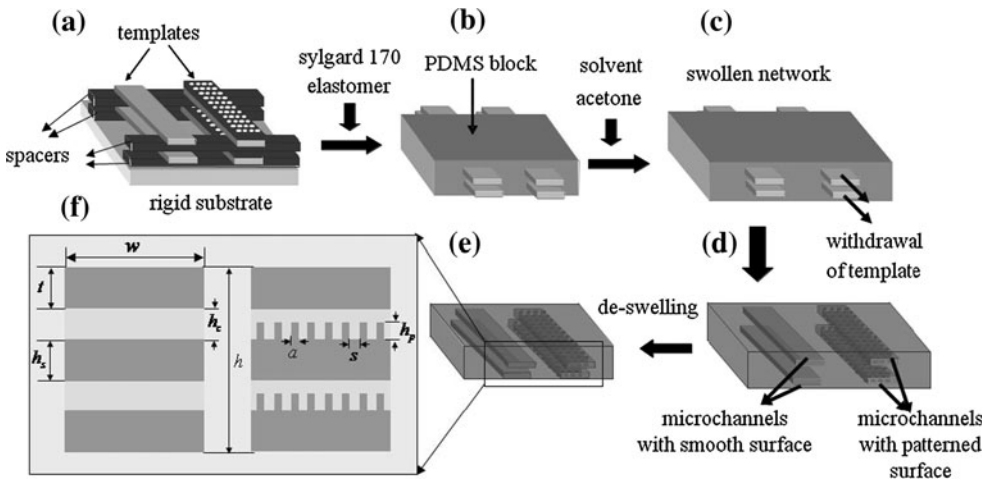

Fig. 2 Preparation of adhesive film embedded with microchannel. **a–e** The diagrams depict the process of generating the stack of microchannels within a block of adhesive. **f** Schematic diagram show the side view of the adhesive film with smooth and textured microchannel walls with its geometric parameters involved in it

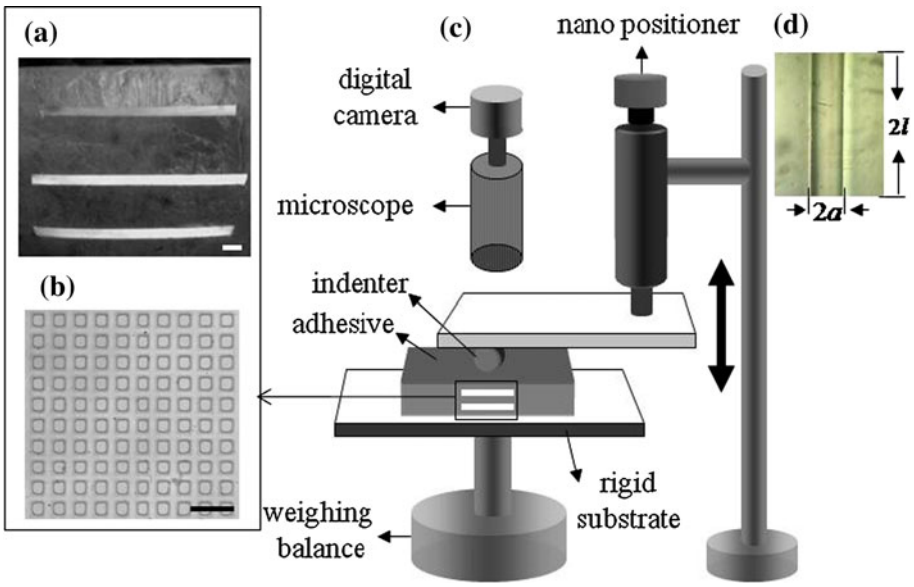

Fig. 3 Schematic of the experiment on adhesive films with embedded microstructures. **a**, **b** The optical microscographs show the side and top views of the adhesive. The scale bar represents 100 μm. **c** Schematic diagram of the experimental setup. **d** An optical micrograph of the area of contact between the indenter and the adhesive film

deionized water and drying by blowing dry nitrogen gas. For complete drying, the samples were kept under low vacuum for 1 h. During this process, the acid hydrolyzes the adhesive surfaces which digest the siloxane bonds and generate silanols which participates in hydrogen bonding [22] with a contacting surface thereby enhancing the surface hysteresis.

Figure 3a shows the side view of a typical crosslinked elastomeric layer of sylgard 170 embedded with three vertically stacked microchannels which span whole through the width of the layer. These channels are rectangular in cross-section with their flat surfaces parallel to that of the adhesive. The inner walls of the microchannels are either smooth or one of their flat surfaces micro-patterned with an array of square pillars as depicted by the top view in Fig. 3b. Figure 3c depicts the experiment in which the adhesive remained bonded to a rigid substrate while a glass hemicylinder of length 2 mm and radius of curvature $r = 2.6$ mm was indented against it at a constant rate 1.5 μm/s. The hemicylinder was axisymmetrically aligned with the channel so that its axis ran parallel to its length; as a result, the contact line propagates along a direction normal to that of the width of the channel (Fig. 3d). The load, P, versus displacement, Δ, plots are obtained in cyclic loading and unloading experiment.

Results and discussions

Adhesive embedded with single layer of microchannel

An estimate of the hysteresis for this adhesive is obtained by calculating the shaded area between the loading and unloading curve and dividing it by the maximum area of contact between the adherents [27, 28]. Curve 1 in Fig. 4a shows the P versus Δ data for a uniform hydrolyzed layer without any internal structures, in which the loading and unloading curves almost superimpose $\Delta E = \oint P\,\mathrm{d}\Delta/A_{\max}$ resulting in $\Delta E_{\mathrm{hyd}} = 92 \pm 14$ mJ/m^2. This value collaborates well with more rigorous adhesive experiments, e.g., JKR contact mechanics experiments [29] performed on similar layers [22]. This smooth and hydrolyzed adhesive layer is considered as the control for comparison with the subsequent experiments.

The curve 2 in Fig. 4a depicts the P versus Δ plot for an adhesive film embedded with a single layer of microchannel with smooth, untextured surfaces. During loading, the indenter first contacts the adhesive surface forming a primary contact area at the interface 1 (optical micrograph A of Fig. 4a). With increased indentation, the indenter presses against a thin film 1–2 of thickness 440 μm which remains supported by the side walls of a microchannel. As a result, the load increases along AB, but with slope smaller than that of curve 1 obtained earlier. At this, the film 1–2 stretches, bends, and eventually contacts with surface 2′ forming secondary contact area as shown in the micrograph B of Fig. 4. Beyond it, the adhesive layer behaves like a single homogeneous block, with its effective shear modulus increased, as evident from increased slope of the B–C portion of the curve 2 in Fig. 4a. During unloading, the curve C–D retraces the loading curve B–C, with decrease in the contact area 2–2′. However, the contact 2–2′ does not detach completely at D, but because of hysteresis it continues to decrease till E. The micrographs E and F of Fig. 4 depict that while the interface 2–2′ detaches, the area of the interface 1 increases. After the complete detachment of interface 2–2′, the area of the interface 1 decreases with unloading of the indenter, until

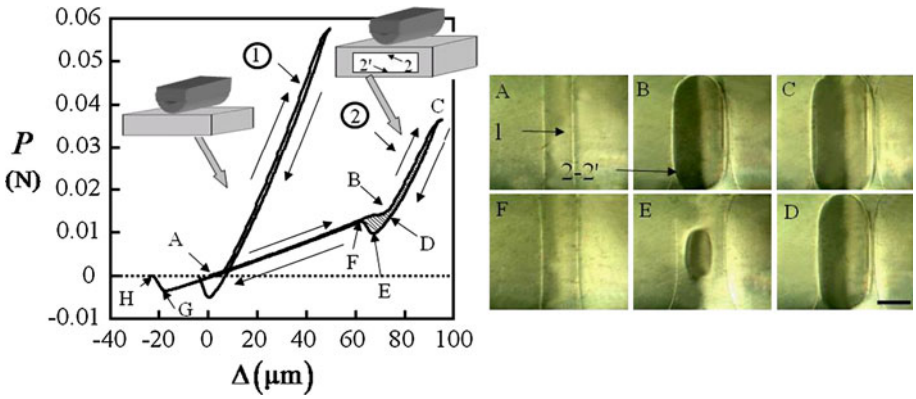

Fig. 4 **a** Curve 1 represents an adhesive layer ($h = 2$ mm) without any internal structures. Curve 2 represents an adhesive with an embedded microchannel ($h_c = 100$ μm, $t = h_s = 440$ μm, and $w = 2$ mm). The shaded area B–D–E–F represents hysteresis during loading and unloading of the indenter. The optical micrographs A–G depict the sequence of events at interfaces 1 and 2–2′ corresponding to curve 2. The scale bar represents 500 μm

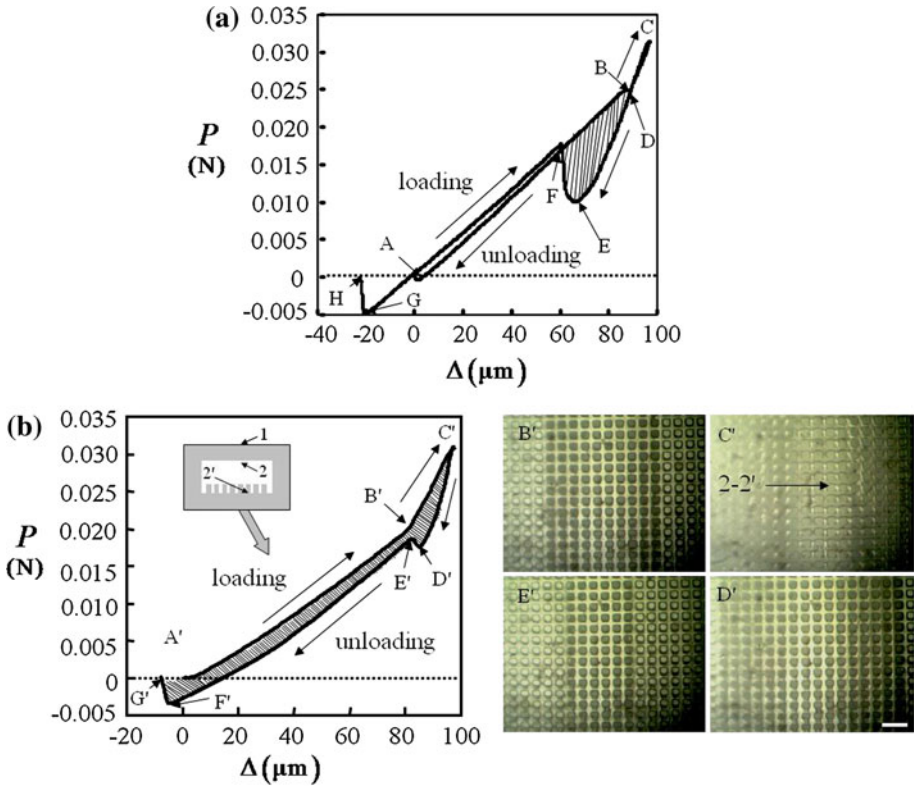

Fig. 5 **a** The load versus displacement plot for an adhesive layer before hydrolysis treatment embedded with a microchannel ($h_c = 100$ μm, $t = h_s = 440$ μm, and $w = 2$ mm) with its surface 2′ patterned with square pillars ($a = 45$ μm, $h_p = 15$ μm, and $s = 42$ μm). **b** The load versus displacement plot for an adhesive layer after hydrolysis treatment embedded with a microchannel ($h_c = 100$ μm, $t = h_s = 440$ μm, and $w = 2$ mm) with its surface 2′ patterned with square pillars ($a = 45$ μm, $h_p = 15$ μm, and $s = 42$ μm). The optical micrographs B′–E′ depict the sequence of events at interface 2–2′. The *scale bar* represents 100 μm

the indenter completely separates from the adhesive surface. The shaded area represents the adhesion hysteresis, which for an indentation depth of $\Delta = 100$ μm, is calculated to be $\Delta E_{hyd} = 238 \pm 17$ mJ/m^2.

Adhesive embedded with single layer of microchannel with textured channel wall

While in the above experiments, the microchannels were smooth walled [21], we now present results in which one of the walls was micro-patterned with square pillars of dimensions $a = 45$ μm, $h_p = 15$ μm, and $s = 42$ μm. Experiments were performed on this film for an indentation depth of $\Delta = 100$ μm for which the hysteresis was calculated to be $\Delta E_{pat} = 310 \pm 52$ mJ/m^2 (Fig. 5a), significantly higher than that for films with untextured microchannels, $\Delta E = 161 \pm 12$ mJ/m^2. A typical video recording of the crack propagation at the internal surface of the microchannel, i.e., at interface 2–2′ shows that in contrast to smooth propagation of crack on untextured surfaces (optical micrographs B–E of Fig. 4a), here the crack initiates from one row of pillars, propagates towards

the next row but eventually gets arrested there till a critical debonding load is reached. This multiple, intermittent crack propagation significantly increases the interfacial self adhesion as observed earlier for surface patterned adhesives [14, 15, 27, 28].

We have integrated the effects of physical patterning with chemical hydrolysis depicted earlier. Figure 5b depicts the load versus displacement plot for indentation experiments with these layers. Curve A′B′C′ denotes the loading data, where the wall of the channel 1–2 first comes into contact with the pillars as apparent from the micrograph B′ of Fig. 5b. With increased loading, the pillars compress and bend and the surface 1–2 eventually contacts the surface 2′ (micrograph C′); at this, the slope of the B′–C′ portion of the loading curve increases. During unloading, the interface 2–2′ separates, but the load versus displacement curve does not superimpose B′–C′ but continues to decrease till D′ (micrograph D′). With further unloading, the debonding between the microchannel wall 1–2 and the surface of the patterns ensues, marked by the slight increase in load as shown by the curve D′–E′. Beyond it, the load decreases continuously with decreases in Δ till the contacting surfaces completely separates as shown by the portion E′–F′ and the corresponding optical micrograph E′. Following this, the portion F′–G′ of the load versus displacement curve denotes the complete separation of the hemicylindrical indenter from the adhesive surface. Thus, hysteresis between the loading and unloading curves is contributed by the following factors: enhanced compliance of the adhesive engendered by the embedded stack of microchannels and the self adhesion hysteresis of the chemically treated surfaces. In addition, for channels with patterned surface, the crack at the interface of the patterns and the microchannel surface 2′ does not propagate continuously but intermittently with "crack arrests and initiations"; this too contributes to the hysteresis. Furthermore, buckling of the pillars under normal load and subsequent straightening during their unloading [30, 31] can too contribute to the intermittent propagation of the crack and the consequent hysteresis.

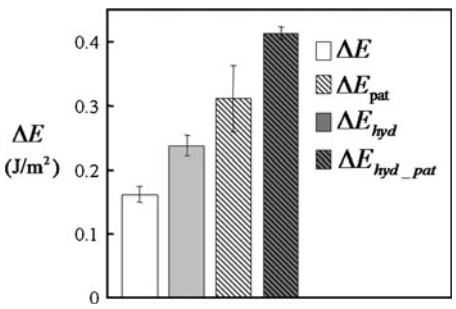

Fig. 6 The bar chart depicts the effect of hydrolysis on the adhesive embedded with microchannel for various cases

The sum-total of all these hysteretic effects for the hydrolyzed film with patterns was found to be $\Delta E_{\text{hyd\_pat}} = 414 \pm 9$ mJ/m^2 which is higher compared to a nonhydrolyzed adhesive film with patterns, $\Delta E_{\text{pat}} = 310 \pm 52$ mJ/m^2. This effect of hydrolysis on the adhesive embedded with microchannel for various cases was depicted in the bar chart of Fig. 6.

Adhesive embedded with a stack of microchannels with textured channel wall

The effects of patterns inside the subsurface are further enhanced by embedding a stack of several layers of such patterned microchannels inside the adhesive film. Figure 7a shows P versus Δ plot for an adhesive film embedded with three layer of microchannel one surface of which, e.g., surfaces 2′, 3′, and 4′ are patterned with the array of pillars having dimensions $a = 67$ μm, $h_{\text{p}} = 15$ μm, and $s = 42$ μm. Here, the indentation is carried out to a sufficient indentation depth, $\Delta = 350$ μm, so that the walls of the microchannel embedded deepest within the adhesive film can self adhere. The loading curve ABCDE of Fig. 7a shows that the channel interfaces 2–2′, 3–3′, and 4–4′ adhere sequentially with corresponding increase in the slope. The micrographs A–E in Fig. 7b picturise how during loading, each microchannel bends and eventually bonds with a surface vertically below. During unloading, these interfaces 2–2′, 3–3′, and 4–4′ of the wall of the microchannels separates resulting in three distinct regimes of hysteresis as shown by the shaded portions in Fig. 7a. Therefore, the cumulative value of this adhesion hysteresis was estimated for an indentation depth $\Delta = 350$ μm and was found to be $\Delta E_{\text{hyd\_pat}} = 1272 \pm 84$ mJ/m^2. The hysteresis, ΔE, increases with both Δ and n till a plateau value, $\Delta E_{\max}$, is reached as shown by the dotted lines in Fig. 8a. Here we have summarized the results of hysteresis for indentation depths up to $\Delta = 350$ μm, which show that beyond $\Delta = 350$ μm the hysteresis values do not alter any significantly, suggesting that the plateau value of the hysteresis is reached at $\Delta = 350$ μm.

We can estimate the differential enhancement in hysteresis associated with the adhesion of only the pillars on the channel surfaces and subsequent debonding as $\lambda = \Delta E_{\max\,\text{pat}} - \Delta E_{\max\,\text{smooth}}$ which is found to increase with the following parameters: number of layers in the stack, the height of the pillars, and the pillar dimensions but it decreases with the inter-pillar distance. As a first approximation, each pillar can be considered as an elastic spring with spring-constant: $K_{\text{s}} = \mu a^2/h_{\text{p}}$ where μ is the shear modulus of adhesive layer. During unloading, the pillars do not separate instantly but follow the upper surface of the channel because of their enhanced compliance. In essence,

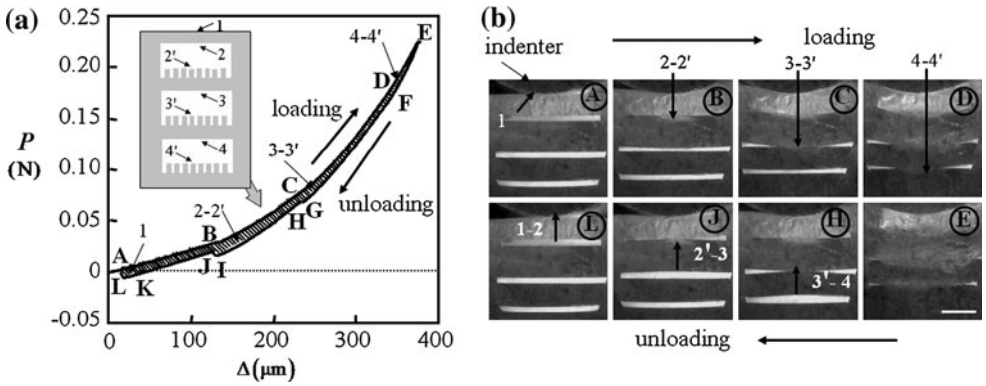

Fig. 7 **a** The loading and unloading data correspond to an adhesive embedded with three layers of microchannels ($t = h_s = 440$ μm, $h_c = 100$ μm, and $w = 2$ mm). Furthermore the channel wall surface 2′, 3′, 4′ are regularly patterned with square pillars ($a = 67$ μm, $h_p = 15$ μm, and $s = 42$ μm). The curve shows three distinct regimes of adhesion hysteresis at interfaces 2–2′, 3–3′, and 4–4′, respectively. **b** Micrographs A–L shows the interfaces corresponding to the displacement, Δ, during loading and unloading experiments. The *arrows* depict the bending effect of internal walls of channels. The *scale bar* represents 500 μm

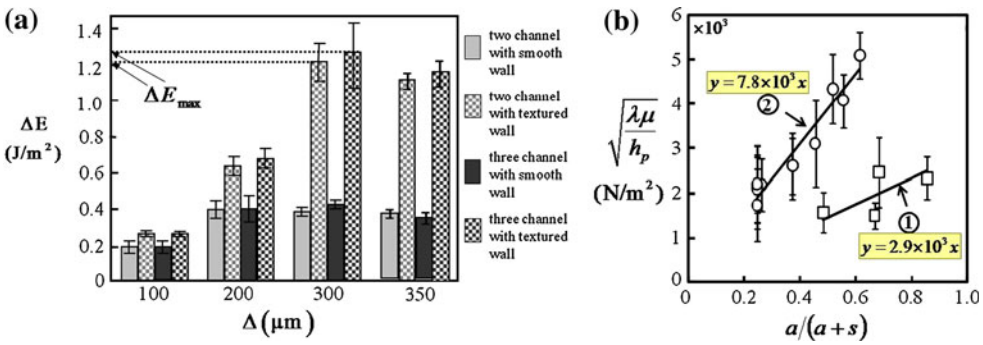

Fig. 8 **a** Plot of ΔE versus Δ for surface patterns having two and three layers of microchannels (square pillars $a = 67$ μm, $h_p = 15$ μm, and $s = 42$ μm). **b** Plot $\sqrt{\frac{\lambda\mu}{h_p}}$ vs. $\frac{a}{a+s}$ for the adhesive film having one layer of microchannel before hydrolysis (curve 1) and after hydrolysis (curve 2)

each spring gets extended till a critical stress level σ_c is reached at which it snaps off the contacting surface of the channel. The critical stretching δ_c at which the pillar snaps off can be expressed as $\delta_c = \sigma_c a^2/K_s$ while the stretching energy stored in the pillar can be written as, $\frac{1}{2}K_s\delta_c^2 = \frac{1}{2}\sigma_c^2\frac{h_p a^2}{\mu}$. While for a smooth continuous layer, the elastic energy is conserved, for the pillar, after snap off it relaxes back at zero load thus dissipating the elastic energy. Thus, each pillar at the contacting area contributes $\sim \frac{1}{2}\sigma_c^2\frac{h_p a^2}{\mu}$ amount of energy to the hysteresis. Since for an adhesive film with a single layer of embedded microchannel, the number of pillars per unit area n_p contributing to the hysteresis can be estimated as $n_p = \frac{1}{(a+s)^2}$, the total energy dissipated because of the pillars is $\lambda = \frac{\sigma_c^2 h_p}{2\mu}\left(\frac{a}{a+s}\right)^2$.

In Fig. 8b, we scale the hysteresis data as $\sqrt{\frac{\lambda\mu}{h_p}}$ and plot as a function of $\frac{a}{a+s}$ which generates a straight line, the slope of which yields an estimation of critical stress σ_c. Curve 1 in this figure represents the data obtained for an adhesive embedded with a layer of patterned microchannel, which was used without the chemical treatment; from the slope of this curve the critical stress can be calculated as $\sigma_{c\_pat} = 4.11 \times 10^3 \mathrm{N/m^2}$. When the same adhesive film was chemically treated, we obtain the curve 2, which yields a larger value of critical stress as $\sigma_{c\_hyd\_pat} = 1.1 \times 10^4 \mathrm{N/m^2}$.

Summary

We have introduced here the design of a novel adhesive which is hierarchically patterned by first embedding stacked microchannels with internally patterned surfaces and then by creating surface active features of molecular length scale via chemical treatment. We have shown that the hierarchical structure enhances the compliance of the adhesive thereby increasing the adhesion hysteresis. In fact the compliance can be varied over a large range by using suitable geometric parameters of the subsurface structures. Adhesion hysteresis is increased further via incorporation of "crack arrest and crack initiation" during adhesion and debonding of the patterned surfaces and also via "self adhesion hysteresis". Thus, the adhesive is truly hierarchical both in geometry and also in principal as it couples

the effect of several mechanisms for enhancement of adhesion hysteresis in an elastic system. It is also possible to generate spatially varying adhesion and in fact, directional adhesion by altering the spatial orientation of the microstructures embedded inside the adhesive layer. The template assisted method adopted here for embedding these structures inside the adhesive layer and patterning their surfaces is novel, simple and easy to implement. We envisage many novel applications of such adhesive materials.

References

1. Scherge M, Gorb SN (2001) Biological micro- and nanotribology: nature's solutions. Springer, Heidelberg, Germany
2. Arzt E, Gorb S, Spolenak R (2003) Proc Natl Acad Sci USA 100:10603
3. Gao H, Yao H (2004) Proc Natl Acad Sci USA 101:7851
4. Hansen WR, Autumn K (2005) Proc Natl Acad Sci USA 102:385
5. Spolenak R, Gorb SN, Gao H, Arzt E (2005) Proc R Soc Lond A 461:305
6. Geim AK, Dubonos SV, Grigorieva IV, Novoselov KS, Zhukov AA, Shapoval SYU (2003) Nat Mater 2:461
7. Gorb SN (2005) Am Entomol 51:31
8. Smith JM, Barnes WJP, Downie JR, Ruxton GD (2006) J Comp Physiol A 192:1193
9. Gorb SN, Jiao Y, Scherge M (2000) J Comp Physiol A 186:821
10. Lee H, Lee BP, Messersmith PB (2007) Nature 448:338
11. Lee H, Dellatore SM, Miller WM, Messersmith PB (2007) Science 318:426
12. Gorb SN, Niederegger S, Hayashi CY, Summers AP, Votsch W, Walther P (2006) Nature 443:407
13. Majumder A, Ghatak A, Sharma A (2007) Science 318:258
14. Ghatak A, Mahadevan L, Chung JY, Chaudhury MK, Shenoy V (2004) Proc R Soc Lond A 460:2725
15. Chung JY, Chaudhury MK (2005) J R Soc Interface 2:55
16. Greiner C, Campo A, Arzt E (2007) Langmuir 23:3495
17. Greiner C, Campo A, Arzt E (2007) Langmuir 23:10235
18. Glassmaker NJ, Jagota A, Hui CY, Kim J (2004) J R Soc Interface 1:23
19. Jagota A, Bennison SJ (2002) Integr Comp Biol 42:1140
20. Thomas T, Crosby AJ (2006) J Adhes 82:311
21. Arul EP, Ghatak A (2009) Langmuir 25:611
22. Chaudhury MK, Weaver T (1996) J Appl Phys 80:30
23. Silberzan P, Perutz S, Kramer EJ, Chaudhury MK (1994) Langmuir 10:2466
24. Choi GY, Kim S, Ulman A (1997) Langmuir 13:6333
25. Greiner C, Arzt E, Campo Ad (2009) Adv Mater 21:479
26. Verma MKS, Majumder A, Ghatak A (2006) Langmuir 22:10291
27. Noderer WL, Shen L, Vajpayee S, Glassmaker NJ, Jagota A, Hui CY (2007) Proc R Soc A 463:2631
28. Glassmaker NJ, Jagota A, Hui CY, Noderer WL, Chaudhury MK (2007) Proc Natl Acad Sci USA 104:10786
29. Johnson KL, Kendall K, Roberts AD (1971) Proc R Soc Lond A 324:301
30. Ghatak A, Das AL (2007) Phys Rev Lett 99:076101
31. Ghatak A, Majumder A, Kumar R (2009) J Roy Soc Interface 6:203